2024 IEEE 27th International Conference on
Intelligent Transportation Systems (ITSC)
September 24- 27, 2024. Edmonton, Canada

Individualizable Risk Assessment Map for Planning Automated Vehicle Behaviors Respecting Perceived Safety

Ji Hwan Park, Yanze Zhang, Wenhao Luo, and Junmin Wang, *Fellow, IEEE*

2024 IEEE 27th International Conference on Intelligent Transportation Systems (ITSC) | 979-8-3315-0592-9/24/$31.00 ©2024 IEEE | DOI: 10.1109/ITSC58415.2024.10919751

***Abstract*— With the continual introduction of various vehicle automation functions and algorithms, the heterogeneity of human, human-machine, and machine autonomy associated with the vehicles on the roads elevates as well. Ensuring vehicles of heterogeneous autonomy to safely and harmoniously share the roads is important for the interests of driving safety, traffic throughput, and human acceptance of autonomy. Particularly due to the wide range of variations in human perceived safety and risk in driving, empowering the vehicle intelligence to accurately understand the perceived risk by other surrounding vehicles is a critical step towards harmonious road sharing. In this paper, we present an individualizable risk assessment model (IRAM) that can empower vehicles to compute the risk maps that individual drivers perceive from the driving behaviors of other surrounding vehicles on a shared road. The IRAM offers a realistic risk assessment map around a vehicle by integrating the relative motions between pertinent vehicles and drivers' perceived safety preferences. A naturalistic human driving dataset, NGSIM, was utilized to evaluate the risk map generation by the proposed IRAM. The IRAM can be used for planning vehicle behaviors, such as its path and motion, that respect the different perceived safety of its surrounding vehicles' human/machine drivers.**

Keywords: risk assessment, risk map, socially-compliant automated driving, harmonious road sharing

I. Introduction

As the development in autonomous driving and driver-assistance vehicles matures, the number of vehicles equipped with various automation systems is expected to increase on roadways [1]–[6]. This will lead to an increase in the heterogeneity of vehicles across different levels of autonomy, varying from human-driven vehicles (HDV) to autonomous vehicles (AV) of SAE Levels 1 through 5 (AVs 1–5) [7]. Additionally, various vehicle manufacturers introduce another dimension of vehicle heterogeneity as the algorithms and behaviors of the same level of automated vehicles differ with manufacturers. The mixture of human-driven and automated vehicles of various levels increases the complexity of the traffic and raises new driving safety challenges.

Different vehicle manufacturers implement their proprietary and oftentimes non-interpretable AI-based decision-making and control algorithms on their AVs1-5 products, thereby rendering dissimilar driving behaviors. AVs 1-5 may drive with egoistic behaviors (e.g., shorter spacing headway and aggressive lane-changing behavior) that are considered physically safe and efficient based on their sensing and actuation abilities, but may pose threats to other surrounding vehicles. This becomes more concerning to vulnerable HDVs and vehicles with low automation levels that are operated by diverse humans including older, physically-challenged, and impaired drivers with a wide range of driving abilities, preferences, and safety perceptions [8]–[10]. Individual vehicle actions perceived as inappropriate or threatening by other surrounding vehicles may induce panic reactions, crashes, and ripple effects that endanger highway traffic.

The increasing challenges related to driving safety necessitate harmonious coordination among vehicles of heterogeneous human/machine autonomy on highways. To enhance driving safety while achieving harmonious coordination among vehicles, risk assessments among vehicles are necessary. By quantitatively assessing how much risk would be imposed on other surrounding vehicles by its planned path and trajectory, an intelligent vehicle could decide whether to maintain its current motion and trajectory plan or adjust its risk-posing behavior accordingly to reduce the imposed risk to others. By enabling the imposed-risk-aware planning for AVs, behaviors of such vehicles may become courteous to the perceived safety of surrounding vehicles, thus increasing the harmony of the group of vehicles traveling together.

To have a meaningful assessment of the risk posed to other road users, developing a model that could reflect an individual driver's perception of risk is essential. Since human drivers have diverse factors that affect their individually perceived risk, a model that can reflect individual perceived risk is necessary to enable harmonious coordination among the road participants. Considering the perceived risk by others in the motion planning and control stages of ego AVs is necessary, as it not only ensures physical safety but also increases public trust and overall acceptance of AVs and enhances the driving experience of heterogeneous participants. For this reason, we present an individualizable risk assessment map (IRAM) that is capable of reflecting individual drivers' safety preferences and can be used for planning an AV's path and trajectory while respecting the perceived safety of surrounding vehicles.

The contributions of this paper are summarized as follows.

1) We propose a realistic risk assessment model incorporating the relative dynamics between the ego vehicle and surrounding vehicles and the fine-tunable individual driver's safety preferences.
2) We illustrate the flexibility of our model across a range of traffic scenarios.
3) Using naturalistic human driving data, the Next Gen-

J. Park and J. Wang are with the Walker Department of Mechanical Engineering at The University of Texas at Austin. Y. Zhang and W. Luo are with the Department of Computer Science at the University of North Carolina at Charlotte. Emails: jihwanpark98@utexas.edu, yzhang94@uncc.edu, wenhao.luo@uncc.edu, jwang@austin.utexas.edu. This work was partially supported by NSF Awards 2312465 and 2312466.

eration Simulation (NGSIM) dataset, we demonstrate the effective representation of our model compared to previous methods to illustrate its realistic usage.

The remainder of the paper is organized as follows. In Section II, we describe related work. In Section III, we introduce the IRAM model formulation. In Section IV, we describe the experiments. Section V presents the experimental results and Section VI provides conclusion and future plan.

II. Related Work

A. Risk Assessment

There have been several previous studies on how surrounding vehicles pose a risk to an ego vehicle and use the risk assessment to adjust the behavior of the ego vehicle to minimize or avoid collision. Wang *et al.* define risk as the probability of other agents entering ellipsoidal space around the ego vehicle [11]. Agents' probabilistic trajectory distributions are incorporated to compute the posed risk values. Woo *et al.* predict the trajectory of a surrounding vehicle to determine the collision risk space posed on the ego vehicle. The risk space is then used to adjust the action of the ego vehicle to minimize its own collision risk [12]. However, this is not as intuitive as how human drivers make decisions since humans also consider how much risk their action (e.g., lane change) would pose to other vehicles.

B. Risk Assessment Map

A risk assessment map on the environment posed by surrounding vehicles was proposed in [13]. The region in which surrounding vehicles intend to occupy was defined and translated into a region of risk with respect to their positions and motions. Due to the presence of occupancy, the ego vehicle ought to respect and avoid such a region of risk to avoid collision with or imposing risk on the vehicle in that region. However, the points in the environment that are used to compute the risk space are treated as stationary, and the motions of surrounding vehicles are not considered in the risk assessment, thereby resulting in an overly conservative or inaccurate risk assessment in dynamic environments such as highway traffic. Similarly, the authors of [12] adopted a potential field method to identify a region of risk space posed on ego vehicles by surrounding vehicles and introduced an adaptive cruise control method to avoid the risk of collision. Similar to our method, defining a map to represent risk information associated with the surrounding vehicles is presented in [14], where a predictive occupancy map (POM) is proposed to estimate risk when an ego vehicle plans several trajectories to make a lane change. Using a risk map integrated with a deep learning method for interactive trajectory prediction is offered in [15]. However, these maps do not consider the relative dynamics between the vehicles. The model presented in [13] can be updated to integrate relative motions between the vehicles to estimate a more realistic risk posed to vehicles.

C. Human perceived safety

The concept of human-perceived safety concerning robots and vehicles is complex and determined by diverse factors, each contributing uniquely to the overall safety perceived by individuals. Researchers have studied to understand and quantify human perceived safety. Nonaka *et al.* have found that physical attributes like the shape and size of robots can affect human perceived safety [16]. In vehicular context, factors that could affect users' perceived safety are the sizes and velocities at which their or surrounding vehicles are operated, and the proximity of surrounding vehicles [17].

III. Risk Assessment Model Formulation

The objective of having a risk assessment model for automated vehicle applications is to quantify the potential risk posed by the ego vehicle to the surrounding vehicles traveling in the vicinity at any instant. The ego vehicle thus can utilize the computed risk region to determine whether its current and/or future planned path and motion respect or violate other road users' perceived safety and adjust its path and motion accordingly if necessary.

A. Individualizable risk assessment model (IRAM)

To enable the ego vehicle of various levels of automation to assess the perceived risk it poses to the surrounding vehicles, we present a risk assessment model by introducing several important improvements from [13]. Such a new model, referred to as the individualizable risk assessment model (IRAM), explicitly considers the motions of relevant vehicles and is capable of representing diverse safety perception by different vehicles/drivers. Throughout the paper, we define i as the ego vehicle that poses risk and j as a surrounding vehicle that perceives risk from i. The IRAM quantifies the risk posed on the surrounding vehicle j by the ego vehicle i as follows:

$$R_{\phi,\theta,i\to j}(q,p_j,v_i,v_j)=\frac{\exp\left(-(q-p_j)^T\phi\Omega(q-p_j)\right)}{1+\exp\left(-\theta v_r^T(q-p_j)\right)}, \tag{1}$$

where $q\in\mathbb{R}^2$ is any point in the planar environment (*e.g.*, a highway), p_j is the center position of the surrounding vehicle j, Ω is the diagonal matrix of the inverse square of the standard deviation, v_i, and v_j are the velocities of the ego vehicle i and surrounding vehicle j, respectively, and $v_r=v_j-v_i$ is the relative velocity between the surrounding vehicle and ego vehicle. The perceived safety parameters ϕ and θ are diagonal matrices of vectors $[\alpha_{long},\alpha_{lat}]$ and $[w_{long},w_{lat}]$ that control the scale and direction of the perceived risk map. The equation consists of the multiplication of two functions. The numerator term is the Gaussian function that measures the magnitude of perceived risk from the center of the surrounding area. The numerator is multiplied by the logistic function that directs the perceived risk region toward the source of risk. In this problem, we assume all the vehicles' perceived safety parameters, positions, and velocities at each time step are known to one another via communications.

Equation 1 considers vehicles as point estimates by only considering their center position, which does not consider the dimension of vehicles. To incorporate the varying size of the vehicles' dimensions, we extend Equation 1 by first

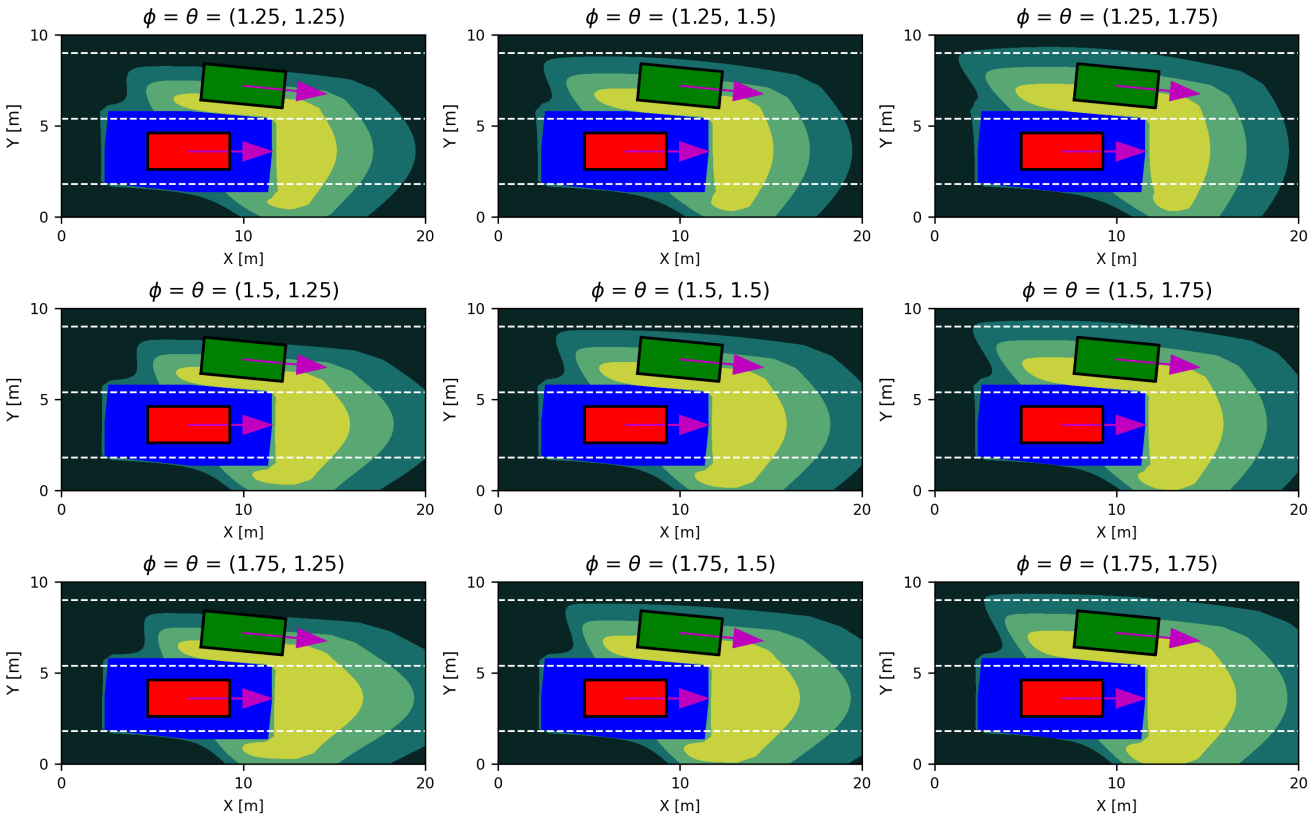

Fig. 1: The effects of varying the parameters ϕ and θ, with values set at [1.25, 1.5, 1.75], are shown. These parameters can alter the size and direction of the perceived risk map for surrounding vehicles. The adjustments in ϕ and θ influence the risk model by shaping the risk contours' spatial and directional characteristics.

defining the effective positions of the ego and surrounding vehicle, positions where the center-to-center distance vector $(q - p_j)$ crosses the edges of the vehicles. These positions inherently include information concerning each vehicle's dimensions of width and length. The effective distance r_{eff} is defined as the relative distance between the ego and the surrounding vehicles' effective positions, $q_{\text{eff}} - p_{j,\text{eff}}$. The effective distance is used to replace $q - p_j$ to utilize a more realistic and accurate distance between two vehicles. The concept of effective distance is illustrated in Fig. 2. Taking account of the dimensions of the vehicles, the physically infeasible region (since two cars cannot overlap with each other) of the potential location of the ego vehicle is presented in blue, as shown in Fig. 1.

$$R_{\phi,\theta,i\to j}(r_{\text{eff}}, v_i, v_j) = \frac{\exp\left(-(r_{\text{eff}})^T \phi \Omega(r_{\text{eff}})\right)}{1 + \exp\left(-\theta v_r^T(r_{\text{eff}})\right)}. \quad (2)$$

B. Relative motion of vehicles

Considering relative motion between vehicles is part of humans' intuitive decision-making process while driving. A human driver typically decides on executing actions such as car following, overtaking, and lane-changing based on their relative motion (how fast or slow their vehicles are compared to other vehicles). Hence, the relative motion between the surrounding and ego vehicles must be incorporated into the risk assessment model, and it influences the risk map by skewing the distribution toward the source of perceived risk.

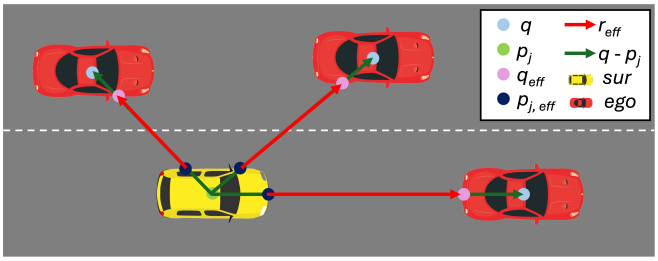

Fig. 2: Effective positions and distance between the ego and surrounding vehicles. The surrounding vehicle and ego vehicles in potential locations are represented as yellow and red, respectively.

C. Perceived safety tuning parameters

The imposed risk by ego vehicle i onto the surrounding vehicle j may be perceived differently with different human drivers or perception systems of vehicle j. Therefore, the tunable perceived safety parameters, ϕ and θ, are incorporated in the IRAM model to reflect various human drivers' safety preferences and/or the differences among vehicle perception systems. In Fig. 3, we demonstrate that our model can recover the model [13] by tuning the parameters ϕ and θ. This flexibility of the IRAM model allows for representations of different perceived safety in the same situation by

choosing different model parameter sets. Additionally, if such an IRAM parameter set of the surrounding vehicle j can be made available to ego vehicle i through, for example, vehicle-to-vehicle (V2V) communication, then ego vehicle i can accurately quantify the risk its path and motion pose on the surrounding vehicle j, thus planning its path and motion respecting such risk, and vice versa, vehicle j can also respect the risk perceived by vehicle i in its planning via $R_{j\to i}$, thereby achieving safe and harmonious road sharing.

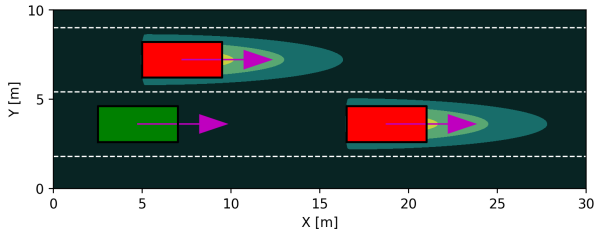

(a) Risk assessment map by [13].

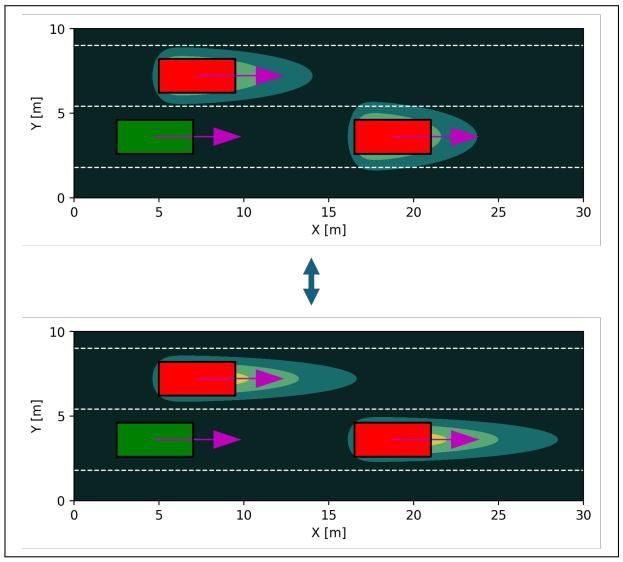

(b) Risk assessment maps by IRAM.

Fig. 3: Ego vehicle: green; surrounding vehicles: red. The parameters ϕ and θ in IRAM can produce different risk assessment map shapes including approximately the same risk map generated by the model in [13]. (a) shows the risk map generated by the model in [13]. (b) shows two cases where the IRAM parameters ϕ and θ are set as [0.8, 1.2], [1.0, 1.4], [1.0, 1.0], [5.0, 1.0] for the above and below, respectively. The IRAM with parameter set of ϕ=[1.0, 1.0] and θ=[5.0, 1.0] can reproduce a similar result as [13].

The sensitivity analysis of these tunable parameters of ϕ and θ is shown in Fig. 1. This demonstration shows how tuning the parameters can affect the size and direction of the posed risk region. As α_{long} or α_{lat} increases, more risk space is formed toward the vehicle's longitudinal or latitudinal direction, respectively. Similarly, as w_{long} or w_{lat} increases, more risk space is skewed toward the vehicle's longitudinal or latitudinal direction, respectively.

D. Physical Interpretation of the IRAM model

We provide an intuitive explanation of the IRAM model to demonstrate how it can be used in diverse driving scenarios. Four commonly encountered driving cases on highways are simulated to illustrate how risk space would form in each case. These cases are vehicle following, smooth lane switching, aggressive lane switching, and lane exchange, which are referred to as Cases 1 through 4 in Fig. 4. The risk maps consist of levels of risk contour where the risk values decrease from the center of the surrounding vehicle. We consider three risk regions: high-risk (yellow), medium-risk (light green), and low-risk (dark green) regions. At each time step, the risk values are computed by sweeping through the map. Every point in the map, q, is considered a potential location, as if the ego vehicle were located at the point with its current motion. In Case 1, the ego vehicle (green) follows the surrounding vehicle (red) with a higher longitudinal velocity. The risk space is formed behind the vehicle, skewed toward the ego vehicle, which is the source of the posed risk. This intuitively makes sense as the drivers perceive risk from tailgating vehicles at higher speeds. Cases 2 and 3 are single-vehicle lane-changing scenarios with an ego vehicle that intends to change into the surrounding vehicle's lane with smooth and aggressive steering, respectively. Due to aggressive steering, which induces higher lateral speed at the instant, a larger risk space is formed toward the lateral direction upward. Similarly, Case 4, which is a two-vehicle lane exchange scenario, induces an even greater difference in relative lateral speed, resulting in greater skewing of the perceived risk direction toward the ego vehicle.

IV. Experiments

We used a naturalistic human driving dataset, NGSIM [18], to evaluate IRAM in highway driving scenarios. The objective is to compare the perceived-risk-violating and perceived-risk-respecting maneuvers of the ego vehicle to demonstrate the effective representation of our model compared to the previous methods and illustrate its realistic usage. We first build a multi-lane highway with five mainline lanes according to the structure described in the NGSIM US-101 dataset. An ego vehicle and surrounding

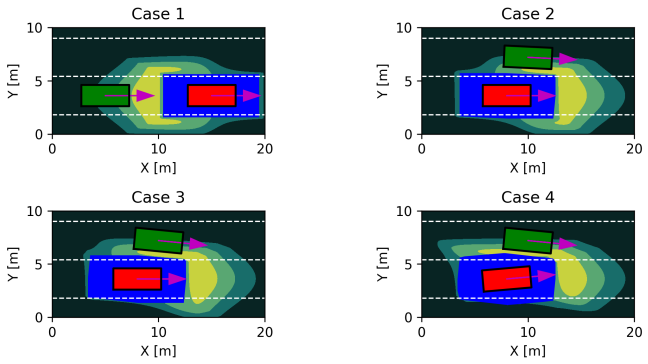

Fig. 4: Four commonly encountered scenarios on highways: Vehicle following (Case 1), Smooth lane switching (Case 2), Aggressive lane switching (Case 3), and Lane exchange (Case 4). ϕ=[1.75, 1.75] and θ=[1.0, 1.5] are selected in this illustration. The risk posed to the surrounding (green) vehicles by the ego (red) vehicle is represented in each case.

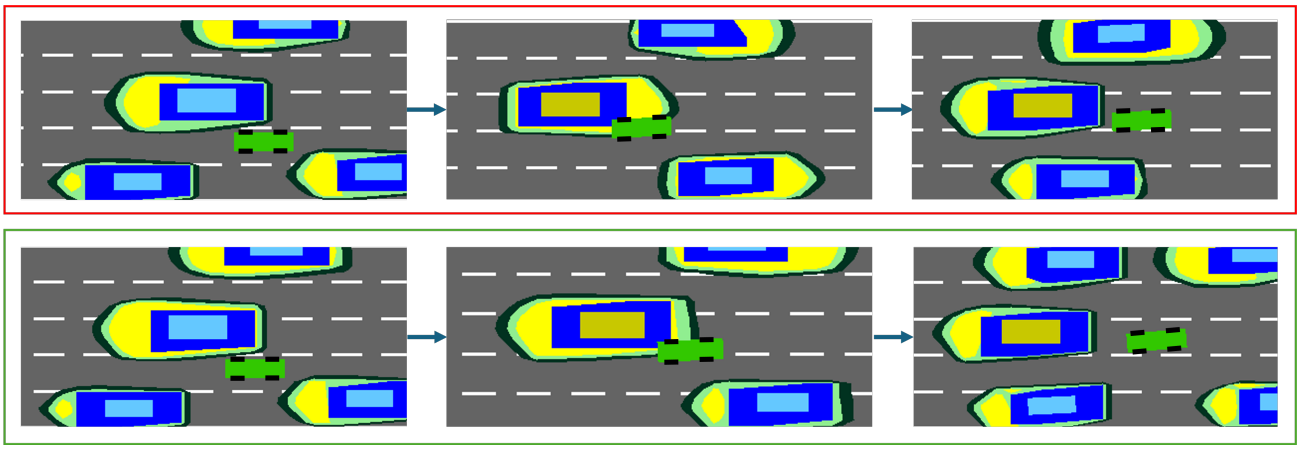

Fig. 5: Risk-violating maneuver (Red upper box) and risk-respecting maneuver (Green bottom box) demonstrations. The ego vehicle, surrounding vehicles, and the vehicle that the ego vehicle is overtaking by changing lanes are represented as green, blue, and dark yellow objects. High, medium, and low-risk levels are yellow, light green, and dark green.

vehicles—vehicles within a 25-meter radius of the ego vehicle—are created on the map. The surrounding vehicles conform to the positions and velocities of the NGSIM, whereas the ego vehicle behaves according to the pure pursuit controller, which creates a target trajectory that the ego vehicle can follow. To demonstrate the potential usage of IRAM, we conduct the experiment with a smooth lane-change scenario. To simulate a lane change in an ego vehicle, we sent a command to the controller to set the target lane to be a lane to the left with a target velocity of 25 m/s and a steering angle of 2.5 ° and 5.0 ° for risk-respecting and risk-violating, respectively. The sampling frequency is set to 20 Hz. In each time step, the perceived risk map of the surrounding vehicles is computed and overlaid on top of the map. The ego vehicle, surrounding vehicles, and the vehicle that the ego vehicle is overtaking by changing lanes are represented as green, blue, and yellow objects in Fig. 5. The perceived risk of surrounding vehicles with our model is represented in red, and the previous model's risk map is presented in purple.

We compare the two maneuvers with three metrics: the time the ego vehicle traveled to complete the lane change, the duration it violated the overtaking vehicle's perceived safety, and the average overlap between the ego vehicle and high, medium, and low-risk regions during the risk violation are computed. We define risk-respecting maneuvers to be ones where the average overlap between is less than 10% across all levels of risk regions. Otherwise, they are considered risk-violating maneuvers. Five simulation trials are completed, and the average value of each metric is reported.

A. Anticipated Collision Time

We use a 2D surrogate safety indicator called Anticipated Collision Time (ACT) which is a generalized Time-To-Collision (TTC) to account for collisions in planar (2D) cases. Although the risk values do not directly represent the ACT, we study how risk values and ACT are correlated to each other as ACT since measuring the time to collision is commonly used as a safety metric. To study the relationship between the risk values and ACT, we randomly sampled three points in each level of risk contour. These points serve as the positions of the ego vehicles and ACT is computed. We removed the points where cars cannot be physically located. The equation to compute ACT is defined as follows:

$$ACT = \frac{\delta}{\left(\frac{d\delta}{dt}\right)}, \tag{3}$$

where δ is the shortest distance between the approaching vehicles at a time instance t and $d\delta/dt$ is the closing-in rate, a rate at which the vehicles approach each other. Further details on computing each variable can be found in [19].

V. Results

A. IRAM Demonstration

The potential usage of IRAM is demonstrated in Fig. 5, where the initial, medial, and final stages of the ego vehicle's lane change behavior are presented. With IRAM, the ego vehicle can determine whether its current trajectory to change lanes respects or violates the other vehicle's perceived risk. In the red upper box, the ego vehicle (green) poses a risk to the surrounding vehicle (yellow) by changing lanes at a relatively higher lateral speed. Hence, it invades the perceived risk region and violates the perceived safety of the surrounding vehicle. In the green lower box, the ego vehicle intends to change lanes with a relatively lower lateral and higher longitudinal speed, which results in a minimal invasion of the perceived risk in front of the surrounding vehicle. Thus, it completed a lane change while respecting the surrounding vehicle's perceived safety with minimal violations.

The quantitative results of the experiment are presented in Table I. Although the risk-violating maneuver completed the lane change faster than the risk-respecting maneuver, it violated the perceived safety of the surrounding vehicle for a longer period of time and in a larger region on average. Hence, the result demonstrates the risk assessment model can

well represent the varying perceived safety of drivers based on ego vehicles' maneuvers. Moreover, the proposed criteria can be used in designing a controller that reduces the time to complete actions such as lane-changing while minimizing the violation time and amount of the violated risk region.

TABLE I: Comparison of risk-respecting and -violating maneuvers.

	Travel time [s]	Violation Duration [s]	High Risk [%]	Medium Risk [%]	Low Risk [%]
Risk-Violating	2.5	1.5	32.5	23.5	21.2
Risk-Respecting	4.8	0.7	3.1	7.2	9.8

B. Correlation between risk values and ACT

The relationship between risk values and ACT is presented in Fig. 6. The correlation between sampled risk values and ACT is computed as -0.8683, strongly suggesting a negative correlation between the two variables. This result is intuitive since the ACT should be higher as the ego vehicle poses a smaller risk with perceived risk-respecting maneuvers, taking a longer time to collide. Thus, the ACT metric serves as a proxy to measure how much the surrounding vehicles perceive risk from the ego vehicle. The strong correlation between the two variables indicates the risk assessment map generated by IRAM represents the individual driver's perceived safety reasonably well.

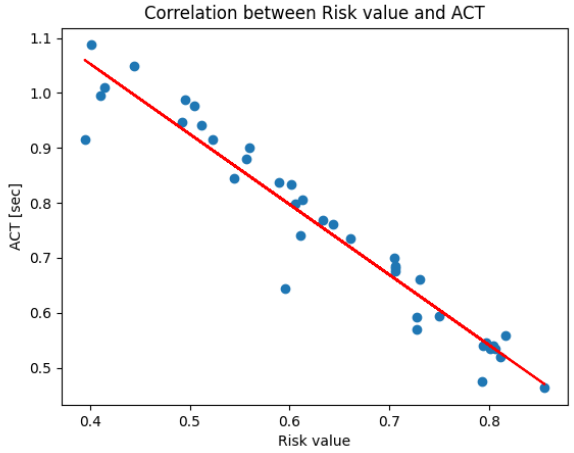

Fig. 6: Correlation between ACT and IRAM estimated risk values.

VI. Conclusions and Future Work

In this paper, we proposed a concept of an individualizable risk assessment model (IRAM) designed to accommodate the different safety perceptions of individual drivers. The integration of perceived safety parameters into the risk assessment model could serve to enhance the path and trajectory planning of automated vehicles by reflecting the perceived safety preference of surrounding drivers. Our result demonstrated a significant correlation between the computed risk values and the anticipated collision time metrics, highlighting the efficacy of IRAM in mirroring individual safety perceptions during highway driving scenarios. For future work, we plan to leverage IRAM to design advanced controllers that not only ensure physical safety but also significantly enhance the overall driving experience for various road users by respecting their driving safety preferences on highways.

References

[1] Y. Chen, C. Hu, and J. Wang, "Motion planning with velocity prediction and composite nonlinear feedback tracking control for lane-change strategy of autonomous vehicles," *IEEE Transactions on Intelligent Vehicles*, vol. 5, no. 1, pp. 63–74, 2019.

[2] J. Wang and R. Rajamani, "Adaptive cruise control system design and its impact on traffic flow," in *2002 American Control Conference*. IEEE, 2002, p. 3690 – 3695.

[3] H. Zhang and J. Wang, "Vehicle lateral dynamics control through afs/dyc and robust gain-scheduling approach," *IEEE Transactions on Vehicular Technology*, vol. 65, p. 489 – 494, 2016.

[4] J. Wang and R. Longoria, "Coordinated and reconfigurable vehicle dynamics control," *IEEE Transactions on Control Systems Technology*, vol. 17, p. 723 – 732, 2009.

[5] K. Bayar, J. Wang, and G. Rizzoni, "Development of a vehicle stability control strategy for a hybrid electric vehicle equipped with axle motors," *Journal of Automobile Engineering, Proceedings of the Institution of Mechanical Engineers*, vol. 226, p. 795 – 814, 2012.

[6] X. Huang and J. Wang, "Real-time estimation of center of gravity position for lightweight vehicles using combined akf-ekf method," *IEEE Transactions on Vehicular Technology*, vol. 63, p. 4221 – 4231, 2014.

[7] O.-R. A. D. O. Committee, "Taxonomy and definitions for terms related to driving automation systems for on-road motor vehicles," SAE International, Tech. Rep., 2021.

[8] S. Schnelle, J. Wang, R. Jagacinski, and H.-j. Su, "A feedforward and feedback integrated lateral and longitudinal driver model for personalized advanced driver assistance systems," *Mechatronics*, vol. 50, p. 177 – 188, 2018.

[9] S. Schnelle, J. Wang, H.-j. Su, and R. Jagacinski, "A personalizable driver steering model capable of predicting driver behaviors in vehicle collision avoidance maneuvers," *IEEE Transactions on Human-Machine Systems*, vol. 47, p. 625 – 635, 2017.

[10] X. Zeng and J. Wang, "A stochastic driver pedal behavior model incorporating road information," *IEEE Transactions on Human-Machine Systems*, vol. 47, p. 614 – 624, 2017.

[11] A. Wang, X. Huang, A. Jasour, and B. Williams, "Fast risk assessment for autonomous vehicles using learned models of agent futures," *arXiv preprint arXiv:2005.13458*, 2020.

[12] H. Woo, Y. Ji, Y. Tamura, Y. Kuroda, T. Sugano, Y. Yamamoto, A. Yamashita, and H. Asama, "Advanced adaptive cruise control based on collision risk assessment," in *2018 21st International Conference on Intelligent Transportation Systems*. IEEE, 2018, pp. 939–944.

[13] A. Pierson, W. Schwarting, S. Karaman, and D. Rus, "Navigating congested environments with risk level sets," in *2018 IEEE International Conference on Robotics and Automation*. IEEE, 2018, pp. 5712–5719.

[14] K. Lee and D. Kum, "Collision avoidance/mitigation system: Motion planning of autonomous vehicle via predictive occupancy map," *IEEE Access*, vol. 7, pp. 52 846–52 857, 2019.

[15] X. Liu, Y. Wang, K. Jiang, Z. Zhou, K. Nam, and C. Yin, "Interactive trajectory prediction using a driving risk map-integrated deep learning method for surrounding vehicles on highways," *IEEE Transactions on Intelligent Transportation Systems*, vol. 23, pp. 19 076–19 087, 2022.

[16] S. Nonaka, K. Inoue, T. Arai, and Y. Mae, "Evaluation of human sense of security for coexisting robots using virtual reality. 1st report: evaluation of pick and place motion of humanoid robots," in *IEEE International Conference on Robotics and Automation, 2004. Proceedings. ICRA'04. 2004*, vol. 3. IEEE, 2004, pp. 2770–2775.

[17] J. A. Thomas and D. Walton, "Measuring perceived risk: Self-reported and actual hand positions of suv and car drivers," *Transportation research part F: traffic psychology and behaviour*, vol. 10, no. 3, pp. 201–207, 2007.

[18] "Next Generation Simulation (NGSIM)," 2016. [Online]. Available: http://doi.org/10.21949/1504477

[19] S. P. Venthuruthiyil and M. Chunchu, "Anticipated collision time (act): A two-dimensional surrogate safety indicator for trajectory-based proactive safety assessment," *Transportation research part C: emerging technologies*, vol. 139, p. 103655, 2022.